

Effect of Sub-energy Windows' Parameters on the Triple Energy Window Scatter Correction Method Accuracy in ^{99m}Tc SPECT Imaging

H. Saikouk^{1,2*}, N. El Khayati¹, A. Matrane²

¹Faculty of Science, Mohammed V University in Rabat, P.O. Box 1014, Rabat, Morocco

²Nuclear Medicine Department, Oncology and Hematology Hospital, Mohammed VI University Hospital, Marrakesh, Morocco

ARTICLE INFO

Article history:

Received 27 January 2021

Received in revised form 24 September 2021

Accepted 13 January 2022

Keywords:

SPECT

GATE

Scatter correction

Triple energy window

ABSTRACT

Scatter correction in SPECT quantification is of major importance to compensation for the scatter contribution under the photopeak. The triple energy windows method (TEW) is one of the suggested ways for scatter correction that are widely used in clinical routine. However, it can be a source of additional noise if the width or the number of sub-energy windows is not accurately chosen. To determine the precise scatter estimation windows settings under the ^{99m}Tc photopeak, scatter fraction was calculated for different sub-energy widths and numbers through GATE Monte Carlo simulation, for a main energy window of 15 %, centered at 140 keV. Four different acquisitions, with cold or hot inserts in a warm or a cold background, were studied. The estimation was done by two methods. The first method was the extraction of the number of detected Compton photons under the photopeak, therefore considered as the true scattered photons. The second method was the application of TEW method to the simulated energy spectra. The comparison of results corresponding to both methods shows a good agreement in two cases: simultaneous 7 % and 5 % sub-energy windows, respectively, positioned on the left and the right of the main energy window, and the second case is a 3 % left sub-energy window without a right sub-energy window. These sub-energy windows were then applied to experimental tomographic acquisitions to assess their impact on contrast, relative noise of the background (RNB), signal-to-noise ratio (SNR), integral uniformity (IU), and tomographic spatial resolution. Good results for these quantitative parameters were acquired with simultaneous 7 % and 5 % sub-energy windows. However, there was very little enhancement for tomographic spatial resolution.

© 2022 Atom Indonesia. All rights reserved

INTRODUCTION

Single-photon emission computed tomography (SPECT) has a limited spatial resolution, which influences the quality of the quantitative studies for scintigraphic images. Compton scattering photons represent one of the major sources of spatial resolution deterioration. It results in loss of contrast and decreases accuracy of quantitative measurements [1].

Hence, several methods had been suggested to compensate for the scatter contribution under the photopeak [2-4]. The triple energy window (TEW) technique is quite popular among these methods [5,6] due to the easiness of its implementation and

its good results. In this technique, scatter estimation is carried out using data acquired in secondary energy windows, abutted to both sides of the main energy window.

However, the choice of the auxiliary energy windows' widths remains an issue for a good estimation of scattering photons' amount [1]. Studies were carried out experimentally [7] and using Monte Carlo simulation [8,9] to evaluate the efficiency of this method, taking into account the choice of the main and sub-energy windows. Some authors recommend the application of narrow sub-energy windows [6], while others suggest using greater widths such as 15 % or 20 % [10].

Given this difference in sub-energy window widths, we decided to investigate the influence of their settings on the estimation of scatter counts under the ^{99m}Tc photopeak. Our aim is to establish

*Corresponding author.

E-mail address: saik.hind@gmail.com

DOI: <https://doi.org/10.17146/aij.2022.1119>

the auxiliary energy windows that permit the most accurate estimation of scatter counts for different sources and phantoms environments.

The study was carried out in two steps. First, Monte Carlo simulations were conducted to determine the accurate scatter fraction for different sub-energy windows' widths and numbers. Second, the secondary energy windows of choice were applied to experimental acquisitions to assess their effect on the quantitative characteristics.

METHODOLOGY

The SPECT system used in this study is Siemens Symbia T6 dual-head SPECT/CT [11], available for routine acquisitions in the Nuclear Medicine Department of Mohammed VI University Hospital. Each head encloses a NaI(Tl) crystal of 3/8 inch thickness, coupled to 59 photomultiplier tubes (PMTs), and a low energy, high resolution, parallel hole collimator (LEHR). The collimator holes' diameter and length are 1.11 mm and 24.05 mm respectively, with septal thickness of 0.16 mm. The field of view (FOV) of the SPECT is 53.3 cm × 38.7 cm.

Simulation setup

A set of simulations were performed, taking into account the Symbia T6 specifics, using Geant4 Application for Tomographic Emission (GATE) [12], a Monte Carlo platform dedicated mainly for the emission tomographic simulations. The purpose of these simulations was to determine the accurate scatter fractions obtained through TEW method, in comparison to those deduced from the detected events under the photopeak, considered as true quantities. Consequently, a validation of our model has been performed beforehand.

Validation setup

Validation of our model was done by comparing the spatial and energy resolution estimated based on simulation with the values obtained experimentally. The simulations were performed for a source-collimator distance of 10 cm and energy of 140 keV. All the acquisitions were performed using an energy window of 15 % centered at 140 keV.

The spatial resolution was determined using a line source of 1.4 mm diameter and 22 cm length, filled with 213.8 MBq of ^{99m}Tc . The source was then positioned in air at 10 cm from the collimator's

external surface, and aligned with the system rotation axis.

Energy resolution of our system was evaluated using a ^{99m}Tc point source, with an activity of 1.295 MBq. The acquisition was performed without the collimator.

Scatter fraction determination

We estimated the values of scatter fraction in tomographic mode instead of planar mode, since it depends on the depth of the source inside the scattering medium [8], and this depth varies for each projection, resulting in a variation of scatter counts throughout the acquired images.

Considering the disparateness of patients' lesions, we performed four tomographic acquisition arrangements: cold spheres in a warm background, hot sources in two different cold backgrounds (air and water), and hot sources in a warm background. For this purpose, we used the following phantoms and sources:

A Jaszczak phantom, where we utilized two of its three parts: the division with cold spheres inserts of different diameters (9.5 mm, 12.7 mm, 15.9 mm, 19.1 mm, 25.4 mm, and 31.8 mm) and the uniform part of 59 mm height above it. The phantom was filled with water mixed to 555 MBq of ^{99m}Tc ;

Hot sources, composed of two syringes of 1 and 10 ml with inner diameter of 4 mm and 16 mm, fully filled with 0.74 MBq and 7.4 MBq of ^{99m}Tc , respectively. Three different backgrounds were probed: in air, in a cylindrical phantom filled with nonradioactive water, and in a cylindrical phantom filled of water mixed with an amount of ^{99m}Tc . For the latter, the source-to-background ratio was 8:1, with a source specific activity of 0.74 MBq/ml.

The energy resolution of our system, 9.9 %, was set in the simulation, and images were acquired with a symmetrical energy window set at 140 keV ± 7.5 %. Tomographic acquisition was performed with 128 projections over 360°, a 128×128 matrix, and 3.3 mm pixel size. The phantoms were aligned with the system axis of rotation, and the acquisitions were performed with a circular orbit of 22 cm radius.

Simulation data outputs were registered and analyzed using ROOT [13], an open-source data analysis framework. The detected events in the energy spectrum, including primaries and scattered photons, were extracted from the ROOT files and used to calculate the scatter fraction SF_G as defined in Eq. (1) for the considered main energy window. SF_G , thus considered as the true scatter fraction, was compared to SF_T (2), the scatter fraction estimated

by applying the TEW method to the simulated energy spectra for different sub-energy windows widths and numbers.

$$SF_G = \frac{C_{SC-G}}{C_{total}} \quad (1)$$

$$SF_T = \frac{C_{SC-T}}{C_{total}} \quad (2)$$

In Eqs. (1,2), C_{total} is the total counts of scattered and unscattered photons in the main energy window, C_{SC-G} is the amount of Compton scattering events in the main energy window, and C_{SC-T} is the total number of scattered photons in the main energy window estimated by TEW, for different sub-energy windows' widths, ranging from 1 % to 20 %.

The triple energy windows method [5] is based on a pixel-by-pixel estimation of scatter counts, C_{SC-T} , by a trapezoidal rule using the following equation:

$$C_{SC-T} = \left[\frac{C_l}{w_l} + \frac{C_r}{w_r} \right] \times \frac{w_m}{2} \quad (3)$$

In Eq. (3), C_l and C_r are total counts at the left and the right sub-energy windows respectively, w_l , w_r , and w_m are the windows' widths for the left and the right sub-energy windows and the main energy window, respectively, as shown in Fig. 1.

In order to increase the detected events and decrease the time consuming simulations, we used the Moroccan grid computing MaGrid [14].

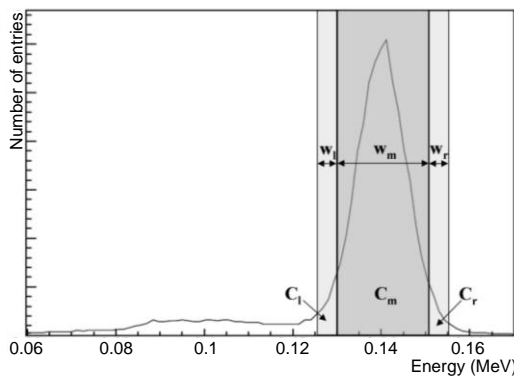


Fig. 1. ^{99m}Tc energy spectrum, with the location and width of the main and sub-energy windows. C_l and C_r are total counts at the left and the right sub-energy windows, w_l and w_r are the widths of the left and the right sub-energy windows, while C_m and w_m are the total counts and the width of the main energy window respectively.

Experimental setup

By considering the simulation results, the accurate values of the sub-energy windows, leading to similar amounts of SF_T and SF_G , were determined. The comparable sets were then applied for scatter

correction in experimental tests in the aim to assess their influence in the quantitative parameters: the contrast, the relative noise of the background (RNB), the signal-to-noise ratio (SNR), the integral uniformity, and the tomographic spatial resolution.

Contrast, SNR, and RNB

Experimental tests were performed under the same conditions as the simulation, detailed in the previous section on scatter fraction determination. A total of 400 000 counts per projection was used, and the uniformity correction was considered during the acquisitions.

The dose calibrator used to measure activities was Scintidose from Lemer Pax. Radiation protection rules adopted in our department and required to manipulate radioactive materials were followed during the measurements. The time of measurement for each dose was recorded, and the residual activities of the empty syringes used to fill the phantoms were measured.

Routine quality controls for SPECT and dose calibrator were carried out before performing the tests.

Image reconstruction was accomplished in the Siemens Syngo workstation using the Flash3D method [15]. The number of iterations was 18 with 8 subsets, and Gaussian filter with spatial resolution of 10 mm was applied. The reconstructed images were corrected for attenuation from CT data by bilinear conversion of Hounsfield Units (HU) into attenuation coefficient at 140 keV [16].

Concerning the scatter correction, the TEW method was applied with the sub-energy windows resulting in a good agreement between SF_G and SF_T estimated from the simulation.

The reconstructed images were analyzed with the AMIDE software package [17]. Circular regions of interest (ROIs) were plotted around the cold spots or the hot spots, with a diameter equal to the physical diameter of the cold spheres and hot syringes, in a stack of five slices, and a 15×15 pixel square ROI was plotted in the uniform part of Jaszczak phantom, as shown in Fig. 2.

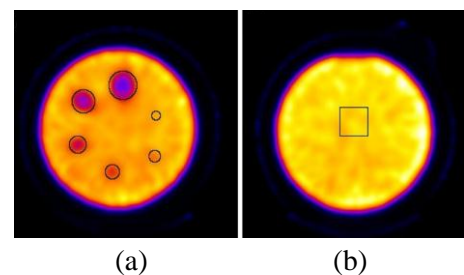


Fig. 2. Examples of ROIs in cold spheres (a), and in the uniform part (b) of Jaszczak phantom.

The statistical results provided by the software were utilized to calculate the contrast for both cold spots C_{cold} and hot spots C_{hot} using Eqs. (4,5) respectively [18].

$$C_{cold} = 1 - \frac{N_{min_cold}}{\bar{N}_{bkg}} \quad (4)$$

$$C_{hot} = \frac{\bar{N}_{hot} - \bar{N}_{bkg}}{\bar{N}_{hot} + \bar{N}_{bkg}} \quad (5)$$

In Eqs. (4,5), N_{min_cold} is the minimum pixel counts in each cold sphere, \bar{N}_{bkg} is the average pixel counts in the background without any insert, and \bar{N}_{hot} is the average pixel counts in the considered hot spot (images acquired with the syringes).

We evaluated the RNB and the SNR using Eqs. (6,7) respectively.

$$RNB = \frac{\delta_{bkg}}{\bar{N}_{bkg}} \quad (6)$$

$$SNR = \frac{|\bar{N}_{spot} - \bar{N}_{bkg}|}{\delta_{bkg}} \quad (7)$$

In Eqs. (6,7), \bar{N}_{spot} is the average pixel counting either in the cold sphere or in the hot spot, and δ_{bkg} is the standard deviation of the background counts.

To estimate the impact of the sub-energy windows widths on the tomographic integral uniformity (IU), we visually investigated the quality of the images, and we calculated its values from the uniform part of Jaszczak phantom by:

$$IU = \frac{N_{max} - N_{min}}{N_{max} + N_{min}} \quad (8)$$

In Eq. (8), N_{max} is the maximum pixel count and N_{min} is the minimum pixel count.

Tomographic spatial resolution

To evaluate the effect of scatter correction on the tomographic spatial resolution, we performed tomographic acquisitions without and with TEW scatter correction for the same sub-energy windows used in the previous section on contrast, SNR, and RNB. For this purpose, we used a line source with a 1.4 mm diameter and 22 cm of length, filled with 55 MBq of ^{99m}Tc , placed at the center of a pile of eight Plexiglas slabs of 7 cm total thickness (3.5 cm above and below the source) used as a scattering medium. Six of the slabs are $30.1 \times 30.1 \times 1 \text{ cm}^3$ in size, when the other two are $30.1 \times 30.1 \times 0.5 \text{ cm}^3$.

The slabs were positioned in such a way as to align the line source with the system central axis, and the acquisition was performed with a circular orbit of 22 cm radius, 128 projections over

360° (64 projections for each head) with 20 000 counts per projection, into a 128×128 matrix and a pixel size of 3.3 mm. For comparison purposes, an acquisition in air has also been performed.

The image reconstruction was executed with the same parameters as for the experimental set-up in the previous section.

The line spread function (LSF), presented as the profile of the counts through the x-axis for transverse reconstructed images, was plotted for each case, and the spatial resolution was expressed as the full width at half maximum (FWHM) of the LSF. Considering that the full width at tenth maximum (FWTM) of the LSF reflects the effect of the scatter on the spatial resolution, this value was also assessed.

RESULTS

Validation

The energy resolution obtained from experiment is $(9.7 \pm 1) \%$ when the value from simulation is $(10.50 \pm 0.07) \%$. Both values are in a good agreement with the manufacturer-recommended value of $(9.9 \pm 1.0) \%$.

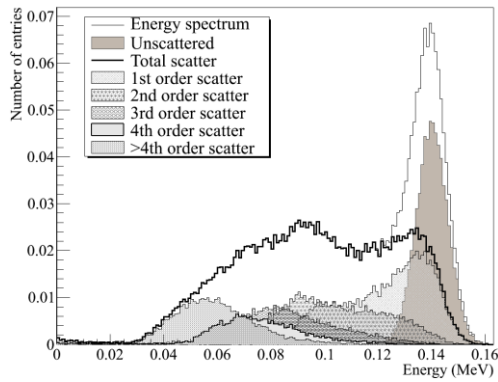
The value of the spatial resolution obtained by simulation is $(0.754 \pm 0.003) \text{ cm}$ and is $(0.785 \pm 0.006) \text{ cm}$ for experiment. Both values are reasonable and in a good agreement with the manufacturer recommended value $(0.74 \pm 0.07) \text{ cm}$.

Scatter order

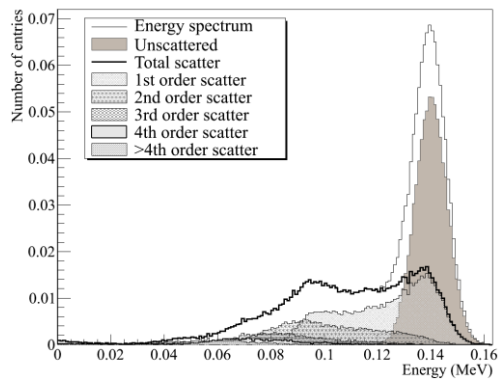
Energy spectra of simulated acquisitions, with detailed scattered photons orders, are shown in Fig. 3. Histograms are normalized such that the sum of weights over all the histogram bins is equal to one. The scattered photons under the photopeak are mainly of first and second orders, when those beyond second order are more predominant in the Compton part of the spectrum where they peak progressively at lower energies.

The tails of the scattered photons distributions extend to high energies. Whereas photons scattering once reach their peak under the photopeak, the tails of photons resulting from two to three successive scattering are also present under the photopeak and are included in the main energy window. On the other hand, the number of photons of second and third orders increases with the presence of a scattering medium.

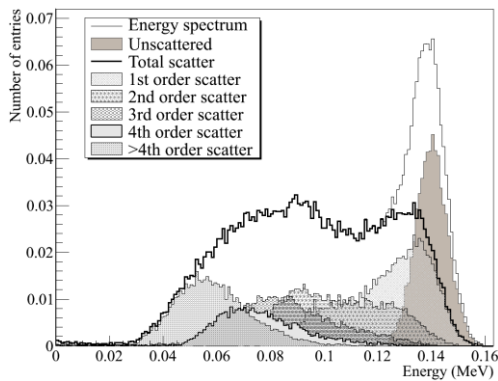
Thus, scatter correction predominantly concerns the elimination of scattered photons of first and second orders counts under the photopeak.



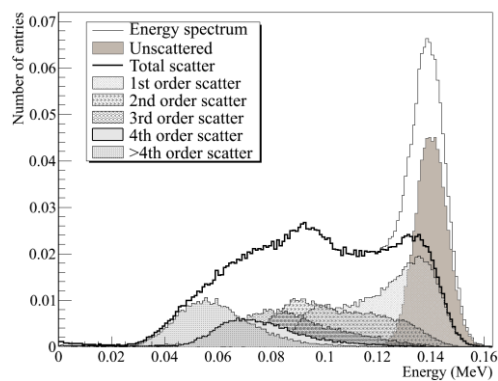
(a)



(b)



(c)



(d)

Fig. 3. Normalized energy spectra from simulation, showing the contribution of scatter orders beyond fourth order, for acquisition (a) with cold spheres inside Jaszczak phantom; and with hot syringes in (b) air, (c) water, and (d) warm background.

Scatter fraction

We calculated the scatter fraction for various sub-energy windows widths, ranged from 1 % to 20 %, positioned on both sides of the main energy window or only on its left.

Comparing SF_G and SF_T , we identified the sub-energy windows which yield to similar scatter fraction values. Table 1 summarizes these results for different acquisitions conditions, including the case of a large sub-energy window, for instance 15 %, actually used for routine tomographic acquisitions in our department.

Table 1. Scatter fraction values evaluated from simulation of four different acquisition conditions, under ^{99m}Tc spectrum photopeak, for a main energy window of 15 %.

Acquisition	SF_G (%)	TEW			
		Two Sub-energy windows (%)	SF_T (%)	One Sub-energy window: $w_r = 0$ (%)	SF_T (%)
Cold spheres	34.5 ± 0.4	$w_l = w_r = 15$	26.3 ± 23.8^a	15	24.4 ± 29.3
		$w_l = 7, w_r = 5$	34.1 ± 1.2	3	34.9 ± 1.2
Hot sources in air	24.9 ± 0.2	$w_l = w_r = 15$	17.4 ± 30.0	15	15.2 ± 39.0
		$w_l = 7, w_r = 5$	25.2 ± 1.2	3	25.1 ± 0.8
Hot sources in water	39.2 ± 0.5	$w_l = w_r = 15$	31.6 ± 19.4	15	29.8 ± 24.0
		$w_l = 7, w_r = 5$	40.6 ± 3.6	3	41.6 ± 6.1
Hot sources in warm background	34.6 ± 0.3	$w_l = w_r = 15$	26.4 ± 23.7	15	24.5 ± 29.2
		$w_l = 7, w_r = 5$	34.1 ± 1.5	3	34.3 ± 0.9

^a: Percentage error from true scatter

A good agreement between SF_G and SF_T was obtained for two sets of sub-energy windows:

- (i) 7 % width at the left side and 5 % width at the right of the main energy window,
- (ii) 3 % width, positioned at the left of the main energy window, when the right sub-energy window is equal to 0.

With large sub-energy windows there is an underestimation of the scatter under the photopeak. Based on the energy spectra from Fig. 3, larger sub-energy windows will result in the inclusion of scattered photons of higher orders in the estimation of scatter fraction, and the increase of percentage error to true scatter. Thus, the use of narrow sub-energy windows is better to estimate scattered photons under the photopeak.

Contrast, RNB, SNR, and tomographic integral uniformity

Experimental images were acquired in the same four different environment as those of the simulation: cold spheres in a warm background, hot spots in a cold background (air or water), and hot spots in a warm

background. Considering the scatter fraction investigation, TEW scatter correction was applied with the sub-energy windows: $w_l = 3%$ ($w_r = 0%$) and simultaneous $w_l = 7%$ and $w_r = 5%$. In addition, and for comparison purposes, scatter correction was applied with the auxiliary windows used actually in our department, *i.e.* $w_l = 15%$, and images without scatter correction were considered as well.

Figure 4 illustrates the effect of scatter correction with three different sub-energy windows in the reconstructed images of the uniform part of Jaszczak phantom. A visual analysis of the images was performed looking for artifacts for each case, and extrinsic uniformity correction was applied to improve the image quality.

Integral uniformity and RNB values are summarized in Table 2. Their quantities are acceptable and within the range of the recommended values [18]. However, the narrow sub-energy window $w_l = 3%$ gave the worst combination of RNB and UI.

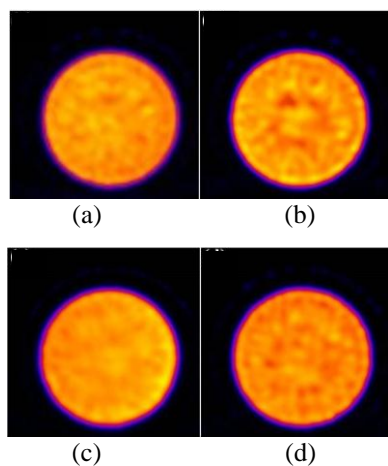


Fig. 4. Reconstructed images of the uniform part of Jaszczak phantom, (a) without scatter correction, and with TEW scatter correction: (b) $w_l = 3%$, (c) $w_l = 15%$ and (d) ($w_l = 7%$, $w_r = 5%$).

Table 2. Tomographic integral uniformity, calculated from the Jaszczak phantom's uniform part, for different scatter correction conditions.

Scatter correction	Sub window width (%)	Integral uniformity (SD) (%)	RNB (%)
No scatter correction	0	12.1 (6.8)	5
TEW (one sub-window)	3	29.1 (5.8)	10
TEW (one sub-window)	15	10.4 (2.6)	3
TEW (two sub-windows)	$w_l = 7,$ $w_r = 5$	19.2 (6.4)	7

In contrast, for a large sub-energy window, *i.e.* $w_l = 15%$ and $w_r = 0%$, the uniformity

value is better and the image is less noisy, hence a better RNB. Without scatter correction the integral uniformity value is still acceptable.

Figure 5 shows the effect of sub-energy windows' widths and numbers in the image quality. For cold sources, five out of the six cold spheres can be seen, and the smallest visible sphere corresponds to 12.7 mm diameter. A good image quality, in comparison to the other images, is observed in the case of $w_l = 7%$ and $w_r = 5%$. The same remark can be observed in the case of hot sources in water and hot sources in a warm background, where the shapes of the spots are better defined than in the other cases.

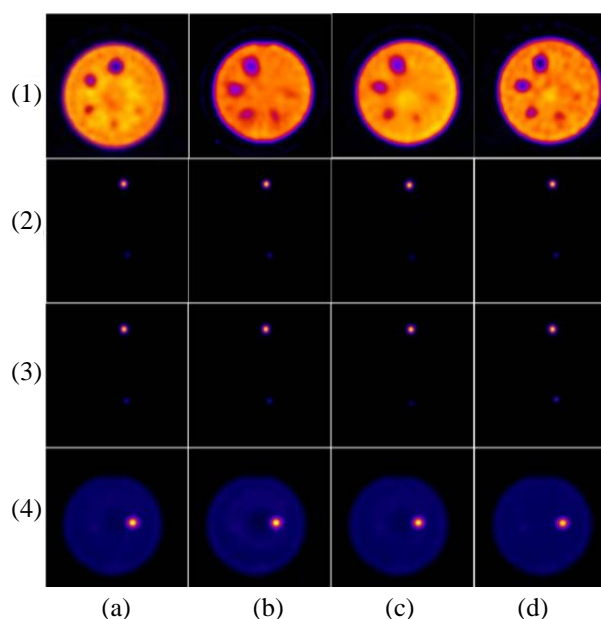


Fig. 5. Transverse reconstructed images of the experimental imaging conditions: (1) the cold spheres, and hot sources (2) in air, (3) in water, and (4) in warm background; (a) without scatter correction; and with TEW scatter correction of (b) ($w_l = 3%$), (c) ($w_l = 15%$), and (d) ($w_l = 7%$, $w_r = 5%$).

We did a quantitative evaluation of the image quality regarding the contrast, RNB and SNR. Table 3 summarizes the obtained results. The contrast values range from 72 % to 87 % in the case of the largest visible cold sphere, and from 20 % to 36 % for the smallest visible cold spot. There was no important difference regarding the contrast values with or without TEW scatter correction. Nonetheless, the noisiest images were obtained with $w_l = 3%$, where the RNB increased by 98 % and the SNR decreased by 47 %.

The average contrast for the case of large hot spot in air is 99.7 %, while it is 96.3 % for the small hot spot. For hot sources in water, the contrast

averages are 99.6 % for the large hot spot and 97.2 % for the small hot spot. In these two cases, air and nonradioactive water, the contrast values were quite similar with a slight difference for small hot spots. Using a warm background with hot sources, the contrast ranges between 82.6 % and 84.0 % for the large hot spot, and from 11.8 % to 15.3 % for the small hot spot. The contrast values were comparable for big hot spots, but there was an improvement of 24 % for the small spot using simultaneous $w_l = 7\%$ and $w_r = 5\%$ sub-energy windows.

Table 3. The values of the contrast, the RNB and the SNR corresponding to different acquisition conditions and sub-energy windows widths.

Acquisition condition	Sub-energy window (%)	Contrast (%)	RNB (%)	SNR	
Cold spheres in warm background	0	85	5	12.6	
	The largest visible spot	$w_l = 3$	86	10	6.6
		$w_l = 15$	72	3.4	17.1
		$w_l = 7, w_r = 5$	87	7.7	8.8
	The smallest visible spot	0	23		3
		$w_l = 3$	36		3
$w_l = 15$		20		4.7	
	$w_l = 7, w_r = 5$	23		2.5	
Hot rods in air	0	99.6		224.2	
	The largest visible spot	$w_l = 3$	99.8		1841.4
		$w_l = 15$	99.6		349
		$w_l = 7, w_r = 5$	99.7		274
	The smallest visible spot	0	97.8		37.5
		$w_l = 3$	98.3		261.8
$w_l = 15$		90.7		11.4	
	$w_l = 7, w_r = 5$	98.6		45.9	
Hot rods in Water	0	99.5		615.2	
	The largest visible spot	$w_l = 3$	99.7		560.6
		$w_l = 15$	99.5		805.1
		$w_l = 7, w_r = 5$	99.8		1961
	The smallest visible spot	0	97		120.9
		$w_l = 3$	97		90
$w_l = 15$		95.5		74.2	
	$w_l = 7, w_r = 5$	99.5		641	
Hot rods in warm background	0	83	3.1	319	
	The largest visible spot	$w_l = 3$	82.6	6.5	145.6
		$w_l = 15$	83.3	3.6	278
		$w_l = 7, w_r = 5$	83.6	2.7	374
	The smallest visible spot	0	12.4		9
		$w_l = 3$	11.8		4.1
$w_l = 15$		12.4		7.9	
	$w_l = 7, w_r = 5$	15.3		13.2	

Without a scattering medium, the contrast and SNR values are optimal for a very narrow sub-energy window, *i.e.* $w_l = 3\%$. Nevertheless, simultaneous $w_l = 7\%$ and $w_r = 5\%$ sub-energy windows in the presence of a scattering medium improve the SNR by up to 219 % and 430 % for big hot spot and for small hot spot in water respectively. This improvement reached 17 % for big hot spot, and 46 % for small hot spot, in a warm background. This enhancement is combined with better RNB values. Our results confirm that TEW method gives better results with hot sources in low-radioactive-background spaces, and that good choice of number

and width of the sub-energy windows improve the scatter correction.

Tomographic spatial resolution

Four LSF were obtained, with attenuation correction, depending on the variation of the sub-energy windows used for the scatter correction. Figure 6 provides the results of these LSF normalized to the maximum counts for each acquisition. FWHM and FWTM values are given in the Table 4. They were assessed with and without attenuation correction.

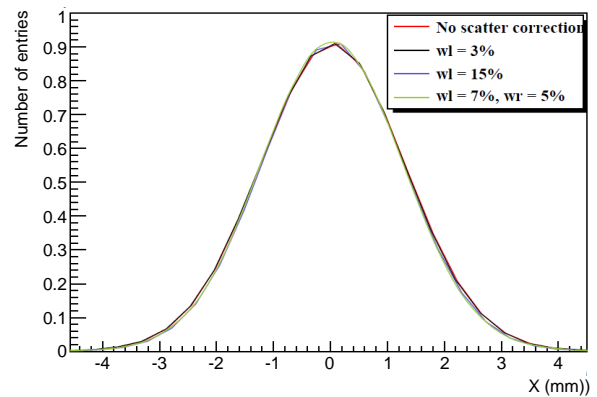


Fig. 6. Experimental LSF through X axis of a line source transverse reconstructed image for different scatter correction sub-energy windows with attenuation correction.

Table 4. Tomographic spatial resolution (SR) values in air and with scattering medium, without and with scatter correction for different sub-energy windows, with (AC) and without attenuation correction (NoAC)

Sub-windows	SR (AC) mm	SR (No AC) mm
In air (0 %)	FWHM : 9.718±0.002	10.714±0.003
	FWTM : 17.712±0.004	19.527±0.006
0 %	FWHM : 9.888±0.001	10.648±0.005
	FWTM : 18.024±0.003	19.407±0.009
3 %	FWHM : 9.867±0.002	10.778±0.007
	FWTM : 17.985±0.004	19.645±0.013
15 %	FWHM : 9.758±0.002	10.630±0.005
	FWTM : 17.786±0.003	19.37±0.01
7 % 5 %	FWHM : 9.746±0.002	10.607±0.006
	FWTM : 17.764±0.003	19.332±0.011

Overall, the combination of scatter and attenuation corrections enhances the FWHM and FWTM values. The latter reflects the scatter contribution in the LSF, and despite the presence of scatter, its values did not change. Hence, the spatial resolution in air did not degrade drastically with the presence of a scattering medium.

DISCUSSION

Triple energy windows method is known as the most accurate scatter correction solution for clinical routine [19]. Nevertheless, choosing the correct width of the main and sub-energy windows remains a dilemma, as a wrong width may lead to an under or an over estimation of scatter counts, thus a wrong estimation of data in the acquired images [1]. Consequently, an erroneous quantification results with noisy images [20,21].

In the present study, we evaluated the accuracy of TEW method in the scatter correction, depending on the choice of sub-energy windows' widths, for a symmetric main energy window of 15 %, centered at 140 keV. The energy spectra separated by scattered photons orders, obtained from Monte Carlo simulation, revealed that the Compton scattered photons of first and second orders are contributing to the formulation of the photopeak. The scattered photons of first order distribution peaks under the photopeak. However, those of upper orders peak progressively toward the lower energies, but tail toward the photopeak, especially scattered photons of second and third orders in the case of acquisition with a warm background. This fact was explained by Floyd *et al.* [8] by the combination of two properties. First, the scattering through small angles results in less energy loss; hence some scattered photons are included in the main energy window. Second, the limitation of SPECT energy resolution leads to the detection of scattered photons with energies as high as those unscattered.

The scatter fraction is an important factor to evaluate the sensitivity of the SPECT system to scattered photons [1]. It depends on the energy resolution and consequently in the main energy window. Nevertheless, a good energy resolution will not result in a low scatter fraction if the choice of the energy window is not correct. On the other hand, the use of a narrow energy window can be useful but will not eliminate scatters of first order since they contribute in the photopeak and tail toward lower energies.

For the main energy window of 15 % used in our routine, scatter fraction (SF) values were estimated from simulation. The SF values vary depending, mainly, on the background, for instance despite of having cold or hot sources in a warm background, the value of SF remains the same. Except with a cold background, the values change and the scatter fraction becomes even more important in water.

A good agreement between GATE and TEW scatter fraction estimation from simulation was obtained in two cases: a 3 % sub window positioned

at the left of the main energy window (the right sub-energy window is equal to 0), and two simultaneous sub-energy windows with 7 % at the left and 5 % in the right of the main energy window. Therefore, narrow sub-energy windows are mandatory to obtain accurate estimation of scatter fraction under the photopeak, especially that wider sub windows lead to the inclusion of scattered photons of higher orders that do not contribute to the scatter under the photopeak. Moreover, a wide sub-energy window results in an underestimation of the scatter counts under the photopeak which influences directly the quantification studies in SPECT.

Several studies [4] showed that for ^{99m}Tc , the use of two sub-energy windows for scatter correction is unnecessary, since the right sub window does not carry significant information about the scattered photons. However, our evaluation proved that the correction with two sub-energy windows, *i.e.*, $w_l = 7\%$ and $w_r = 5\%$, can enhance the image quality quantitatively, especially with the presence of a hot background, or a cold scattering medium, water for instance, where it results in fewer noise, but better contrast, uniformity and SNR, which is the aim of any optimization study. In the other hand, much narrower sub-energy window, *i.e.*, $w_l = 3\%$ and $w_r = 0\%$, can lead to better contrast for cold spheres or hot source in air, nevertheless it degrades the SNR and increases the RNB.

The lower impact of scatter correction in the case of cold spheres in a radioactive background can be explained by the fact that TEW method has larger errors in cold regions than with hot spots in a warm background [9].

Without the scatter correction, the obtained results were acceptable, but the improvement factors can reach 400 % for SNR with the scatter correction.

Spatial resolution is an important factor in SPECT quantification. However, it can be degraded due to multiple factors, such as scatter and attenuation.

In a previous work [22] we concluded that the spatial resolution is more influenced by the scattering medium thickness, the distance source-collimator and whether there is more contribution from back or forward scattering. In the present work we assessed the effect of scatter correction on the tomographic spatial resolution, depending on the sub-energy windows widths used for this purpose. Since the effect of scatter on the spatial resolution is assessed from the FWTM values [1], we concluded from the obtained values that the scatter correction has a little effect on the values of the FWTM. This finding can be justified by the fact that, for the same distance source-collimator, the response has not been significantly affected by scatter since the

FWTM values were not larger than $1.86 \times \text{FWHM}$ as suggested in [1]. Hence the system spatial resolution was not degraded and no scatter correction was necessary.

CONCLUSION

The purpose of the present study was to improve the quality of tomographic reconstructed images, by investigating the influence of the widths and numbers of sub-energy windows in the accuracy of the triple energy windows scatter correction method.

We observed that a large sub-energy window such as 15 % actually used in our department gave acceptable results for the quantitative parameters assessed in our work.

Nevertheless, narrower sub-energy windows improved the image quality and enhanced its parameters, especially the simultaneous $w_l = 7\%$ and $w_r = 5\%$, positioned on either side of the 15 % main energy window.

The next step of our work is to validate and determine the final sub-window that would be used in our department, by applying our results to clinical cases.

ACKNOWLEDGMENT

This research was supported through computational resources of MaGrid (www.magrid.ma) provided by the National Center for Scientific and Technical Research (CNRST), Rabat, Morocco

AUTHOR CONTRIBUTION

All authors equally contributed as the main contributors of this paper. All authors read and approved the final version of the paper.

REFERENCES

1. Quantitative nuclear medicine imaging concepts, requirements and methods, IAEA Human Health Reports No. 9, © IAEA, Vienna (2014).
2. B. F. Hutton, I. Buvat and F. J. Beekman, *Phys. Med. Biol.* **56** (2011) R85.
3. K. F. Koral, X. Q. Wang, W. L. Rogers *et al.*, *J. Nucl. Med.* **29** (1988) 195.

4. A. Kojima, A. Tsuji, Y. Takaki *et al.*, *Ann. Nucl. Med.* **6** (1992) 153.
5. K. Ogawa, Y. Harata, T. Ichihara *et al.*, *IEEE Trans. Med. Imaging* **10** (1991) 408.
6. K. Ogawa, *Ann. Nucl. Med.* **8** (1994) 277.
7. A. Kojima, M. Matsumoto and M. Takahashi, *Ann. Nucl. Med.* **5** (1991) 139.
8. C. E. Floyd, R. J. Jaszczak, C. C. Harris *et al.*, *Phys. Med. Biol.* **29** (1984) 1217.
9. Y. Narita, S. Eberl, H. Iida *et al.*, *Phys. Med. Biol.* **41** (1996) 2481.
10. V. Changizi, A. Takavar, A. Babakhani *et al.*, *J. Appl. Clin. Med. Phys.* **9** (2008) 136.
11. Symbia T Series: System Specifications, Siemens AG (2013).
12. K. Assié, I. Gardin, P. Véra *et al.*, *Phys. Med. Biol.* **50** (2005) 3113.
13. R. Brun and F. Rademakers, *ROOT - An object oriented data analysis framework*, Proceedings AIHENP'96 Workshop, Lausanne, *Nucl. Inst. Meth. in Phys. Res. A* **389**(1997) 81.
14. C. El Amrani, O. Bouhali and R. Merrouch, *IADIS IJCSIS.* **4** (2009) 85.
15. E. Hawman, A. H. Vija, R. Daffach *et al.*, *Flash 3D Technology: Optimizing SPECT Quality and Accuracy*, Whitepaper Flash 3D, Siemens Medical Solutions (2003) 1.
16. J. S. Fleming, *Nucl. Med. Commun.* **10** (1989) 83.
17. A. M. Loening and S. S. Gambhir, *Mol. Imaging* **2** (2003) 131.
18. L. S. Graham, F. H. Fahey, M. T. Madsen *et al.*, *Med. Phys.* **22** (1995) 401.
19. A. Seret, D. Nguyen and C. Bernard, *EJNMMI Res.* **2** (2012) 1.
20. H. Zaidi, *Monte Carlo Modeling in Nuclear Medicine Imaging*, Quantitative Analysis in Nuclear Medicine Imaging, H. Zaidi (Ed.), Springer US, New York (2006) 358.
21. M. N. Asl, A. Sadremomtaz and A. Bitarafan-Rajabi, *J. Med. Phys.* **38** (2013) 189.
22. H. Saikouk and N. El Khayati, *Monte Carlo Simulation of Scatter Effect for Clinical Gamma Camera*, Proceedings of Middle East Conference on Biomedical Engineering, IEEE Computer Society **14** (2014) 30.